InAs quantum dots: Predicted electronic structure of free-standing versus GaAs-embedded structures

A. J. Williamson and Alex Zunger
National Renewable Energy Laboratory, Golden, Colorado 80401
(Received 22 October 1998)

Using an atomistic pseudopotential approach, we have contrasted the (i) strain profiles, (ii) strain-modified band offsets, (iii) energies of confined electrons and holes, and (iv) wave functions and Coulomb interactions between electrons and holes for three types of InAs quantum dots: (a) a free-standing spherical dot, (b) a GaAs-embedded spherical dot, and (c) a GaAs-embedded pyramidal dot. A comparison of (a) and (b) reveals the effects of strain, while a comparison of (b) and (c) reveals the effects of shape. We find that the larger band offsets in the ''free-standing'' dots (i) produce greater quantum confinement of electrons and holes and (ii) act to confine the wave functions more strongly within the dot, resulting in larger electron-hole Coulomb energies. The lower symmetry of the pyramidal dot produces a richer strain profile than the spherical dots, which splits the degeneracy of the hole states and polarizes the emitted light. [S0163-1829(99)02323-1]

I. INTRODUCTION

There are currently two leading methods for producing nanometer size semiconductor quantum dots. The first involves the controlled ripening of a lattice mismatched film, also called ''self-assembled,'' Stranski-Krastanow (SK) growth.[1] In this approach the quantum dot material is deposited on top of a substrate with a different lattice constant, and the resulting strain induces three-dimensional island growth. The most successful systems for producing high quality samples of these SK dots are InAs/GaAs[2,3] and InP/GaInP,[4] which produce approximately pyramidally shaped, coherently strained dots with less than 10% size fluctuations. The second method of fabrication uses colloidal chemistry techniques[5,6] to produce nearly spherical, strain free dots whose surfaces are passivated by organic molecules. These colloidal techniques have recently enabled the production of high quality quantum dots, made from CdSe,[7] CdS,[8] InP,[9] and InAs,[10] all with narrow ($<5\%$) size distributions. Thus, the dots produced by these two methods (SK and colloidal) differ in shape (pyramidal vs spherical), strain (inhomogeneously strained vs unstrained), and barrier height (InAs/GaAs barrier of ~ 0.2 eV vs a few eV barrier in free-standing dots).

Spectroscopic studies on these two types of dots [SK (Refs. 2 and 4) and colloidal[7–10]] have produced several interesting features, but unfortunately, no attempt has been made to compare and contrast their electronic structure in terms of their different (i) shape, (ii) strain, and (iii) band offsets. In this paper we present a theoretical comparison of the electronic structure of these two types of quantum dots. We use InAs embedded in GaAs and free-standing InAs as our model systems. To isolate the physical effects we have studied (a) spherical free-standing InAs dots and (b) spherical InAs dots embedded in GaAs. To see the effect of changing the shape of the embedded dot from a sphere to an idealized pyramidal shape we have also studied (c) a pyramidal InAs dot embedded in GaAs.

II. APPROACH

We use the same pseudopotential Hamiltonian to model the single-particle electronic structure of all three of the above systems,

$$\hat{H} = -\frac{1}{2}\nabla^2 + \sum_{\alpha,n} v_\alpha(\mathbf{r} - \mathbf{R}_{\alpha n}) + v_\alpha^{(SO)}. \tag{1}$$

We expand the single-particle wave functions, ψ_i, in a plane-wave basis

$$\psi_i(\mathbf{r}) = \sum_{\mathbf{G}}^{E_{cut}} c_{\mathbf{G},i}\, e^{i\mathbf{G}\cdot\mathbf{r}}. \tag{2}$$

The matrix elements of the Hamiltonian in Eq. (1) in the basis of Eq. (2) are calculated according to

$$\hat{H}_{\mathbf{G},\mathbf{G}'} = \frac{1}{2}\mathbf{G}^2\delta_{\mathbf{G},\mathbf{G}'} + V_{local}(\mathbf{G}-\mathbf{G}') + V_{nonlocal}(\mathbf{G},\mathbf{G}'). \tag{3}$$

The spin-orbit interaction is represented by a nonlocal pseudopotential $V_{nonlocal}^{(SO)}$, which is evaluated in real space using the linearly scaling small box method from Ref. 11.

The pseudopotential in Eq. (1) is constructed from a sum of screened atomic pseudopotentials v_α, where α represents In, Ga, and As, and $\mathbf{R}_{\alpha n}$ are the positions of the In, Ga, and As atoms within the dot and surrounding barrier material. These positions can be either strained, or strain free (see below). The pseudopotentials v_α are fit in reciprocal space to the functional form

$$v_\alpha(q) = [1 + a_{4\alpha}\mathrm{Tr}(\epsilon)]\,\frac{a_{0\alpha}(q^2 - a_{1\alpha})}{a_{2\alpha}e^{a_{3\alpha}q^2} - 1}. \tag{4}$$

In the fitting procedure, first $a_{4\alpha}$ is fixed and the parameters $a_{0\alpha}$, $a_{1\alpha}$, $a_{2\alpha}$, and $a_{3\alpha}$ are adjusted to fit the experimental (i) full-zone band structure, (ii) effective masses for electrons and holes, (iii) local density approximation (LDA) calculated band offsets and (iv) deformation potentials for electrons and

TABLE I. Fitted parameters for the screened atomic pseudopotentials in Eq. (4).

Parameter	In	Ga	As (InAs)	As (GaAs)
α_0	202.622	123090	93.0562	12.3009
α_1	1.88308	2.27012	2.61982	2.88500
α_2	5.05163	3210.12	1.97179	1.15083
α_3	0.488110	0.624885	0.693073	0.260647
α_4	1.336189	1.629544	0.0	0.0

holes. Then the additional multiplicative factor $[1+a_{4\alpha}\mathrm{Tr}(\epsilon)]$ is included to explicitly introduce strain dependence into the pseudopotential. We find that adjusting $a_{4\alpha}$ in this term allows the *absolute* LDA deformation potentials of the Γ_{15v}, Γ_{1c}, and X_{1c} states of bulk InAs and GaAs to be fitted. Without such a strain dependent term, only the *relative* deformations of $(\Gamma_{1c}-\Gamma_{15v})$ and $(X_{1c}-\Gamma_{15v})$ can be fit. Note, this trace term is not required in a self-consistent calculation. It is crucial in a non-self-consistent calculation to simulate the effects of the changes in the atomic positions on the potential.

In the InAs/GaAs heterostructures studied here, the strain dependence of the band offsets strongly effects the electron and hole confinement energies and it is therefore essential to accurately reproduce the *absolute* deformation potentials of the individual bands. In Eq. (4), $\mathrm{Tr}(\epsilon)$ is defined as $\Omega(\mathbf{R})/\Omega_0$, where $\Omega(\mathbf{R})$ is the volume of the tetrahedron formed by the four nearest neighbors of the atom at $\mathbf{R}$ and Ω_0 is the volume of the same tetrahedron in the unstrained bulk. The fitted values of $a_{0\alpha}$, $a_{1\alpha}$, $a_{2\alpha}$, $a_{3\alpha}$, and $a_{4\alpha}$ are given for the InAs dot material and the GaAs barrier material in Table I. Note that the $a_{4\alpha}$ parameter is set to zero for As to avoid any ambiguity due to shared As atoms at InAs/GaAs interfaces.

For each system we construct a supercell containing the InAs dot with a chosen shape and a surrounding ''barrier material.'' For the embedded dots this barrier material is GaAs, while for the free-standing dot we passivate the surface dangling bonds by pseudoatoms representing a fictitious material with a very large band gap, designed to mimic the effects of vacuum. This artificial material is fitted to have the same lattice constant as InAs, so no strain is introduced into the system. In the GaAs-embedded InAs dot systems there is a 7% lattice mismatch between GaAs and InAs, so the atomic positions are first relaxed to their minimum strain energy values, using the valence force field (VFF) elastic energy functional[12] before calculating the electronic structure. The VFF functional used in this work[13] is based on Martin's[14] generalization of the Keating potential to heteropolar semiconductor systems. The agreement between VFF energies and first principle determined energies was tested by Silverman *et al.*[15] for GaP-InP and found to be very satisfactory. In each system the supercell is periodically repeated, to enable the use of standard band-structure techniques. This periodic repetition can introduce spurious interactions between neighboring supercells. These interactions may take the form of either an electronic coupling between the wave functions of the dots in adjacent supercells or a coupling of the strain fields in adjacent cells. In the present calculations, sufficient barrier material was used to ensure that both types of interaction were negligible. We test the convergence of the electronic properties with respect to supercell size by repeating the calculations in supercells whose size is increased by 22.9 Å . This increase altered the absolute single particle energies by less than 10 meV and the energy splittings by less than 2 meV. The three systems studied in this paper are (a) a spherical free-standing $In_{736}As_{683}$ dot with 42.2 Å diameter (b) the same spherical dot embedded in GaAs, and (c) a pyramidal $In_{770}As_{886}$ dot, with 30.3 Å height and 60.6Å base and {101} facets, embedded in GaAs.

The supercells contain up to 30 000 atoms, which is too large for the Hamiltonian in Eq. (1) to be solved by direct diagonalization. We thus use the ''folded spectrum method'',[16,17] in which one solves for the eigenstates of the equation

$$(\hat{H}-\epsilon_{ref})^2\psi_i=(\epsilon-\epsilon_{ref})^2\psi_i, \tag{5}$$

where ϵ_{ref} is a reference energy. By placing ϵ_{ref} within the gap, and close to the valence-band maximum or conduction-band minimum, one is then able to obtain the top few valence states or the bottom few conduction states, respectively. As quantum confinement effects act to lower (raise) electron (hole) levels in the dot compared to the bulk, one can ensure ϵ_{ref} falls within the band gap of the dot by placing it within the bulk band gap of the dot material (in this case InAs).

III. RESULTS

A. Strain profiles

Before discussing the detailed electronic eigenstates of the dots, we first examine their strain profiles and the resulting strain-modified band offsets. As will be shown below, these provide a useful basis for analyzing the details of the resulting eigenstates. The strain ϵ_{ij} is defined as in Ref. 13,

$$\epsilon_{ij}=R'_{ij}R_{ij}^{-1}-I, \tag{6}$$

where R_{ij} is a matrix containing three of the unrelaxed tetrahedral bond vectors, R'_{ij} contains the same vectors after VFF relaxation, and I is the unit matrix. The shear strain components are one to two orders of magnitude smaller, and have little effect on the electronic structure. In Fig. 1 we plot the diagonal components of the VFF calculated strain profile along the [001] direction through the center of (a) the GaAs-embedded spherical InAs dot and (b) the GaAs-embedded pyramidal InAs dot. The strain components $\epsilon_{xx}, \epsilon_{yy}$, and ϵ_{zz} correspond to strain along [100], [010], and [001], respectively. The strain profile of the embedded spherical dot (a) is qualitatively the same as that predicted by Eshelby[18] for an isotropic spherical inclusion embedded in an isotropic matrix: The InAs dot is uniformly compressed (3.5%), while the

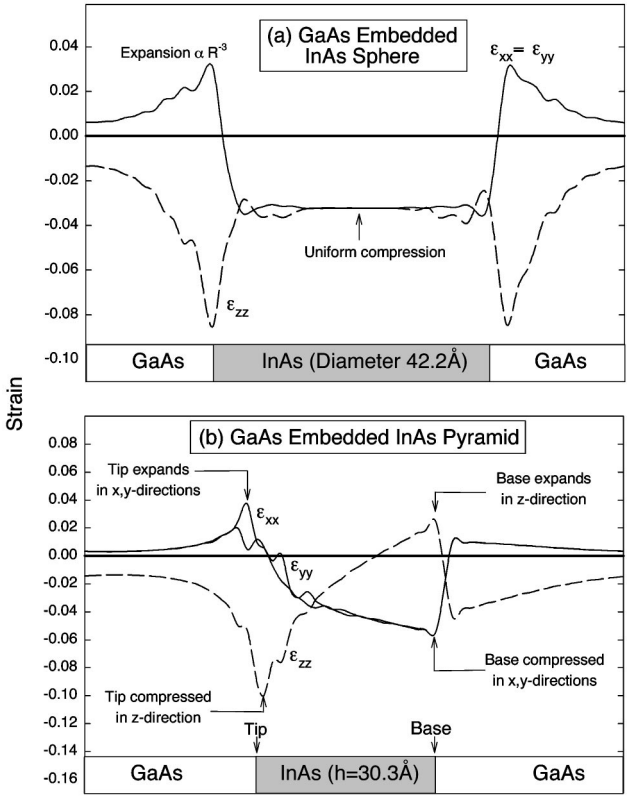

FIG. 1. Diagonal components of the strain along the [001] direction through the center of the GaAs-embedded (a) spherical InAs dot with 42.2 Å (diam) and (b) pyramidal InAs dot with 30.3 Å height and 60.6 Å base. The *x*, *y*, and *z* directions are along [100], [010], and [001], respectively. Negative (positive) strain corresponds to compressive (tensile) strain.

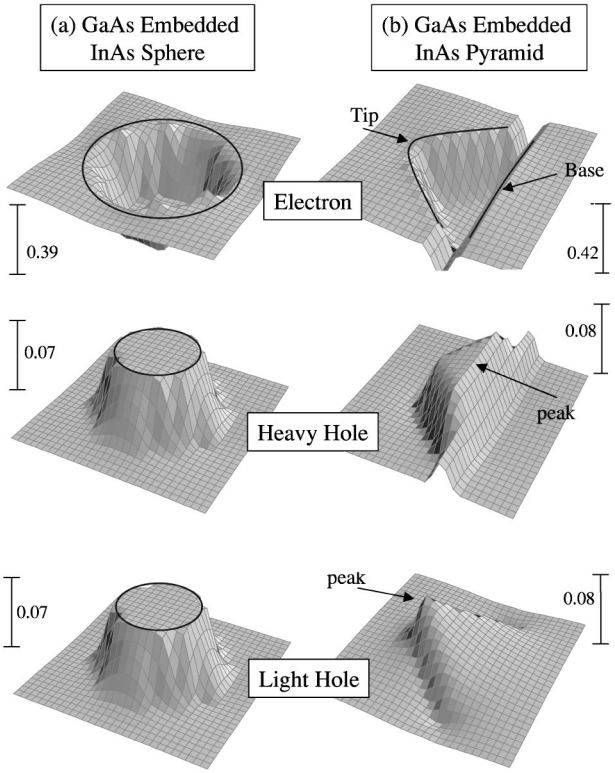

FIG. 2. Strain modified electron, heavy-hole, and light-hole potential offsets in the {010} plane through the center of the GaAs-embedded (a) spherical InAs dot with 42.2 Å diameter and (b) pyramidal InAs dot with 30.3 Å height and 60.6 Å base. The scale bars show the maximum depth of the electron and hole wells in eV. The black lines mark the approximate edges of the electron and hole wells. These model calculations are illustrative ones based on the model Eqs. (7) and (8). They are completely separate from the solutions presented in Fig. 3 which are eigenstates of the Hamiltonian in Eq. (1).

GaAs matrix is compressed in the direction perpendicular to the interface with the dot (ϵ_{zz}), and expanded in directions parallel to the interface ($\epsilon_{xx}, \epsilon_{yy}$). The strain profiles in the GaAs matrix decay by approximately[18] $1/R^3$, where R is the distance from the center of the dot. The lower symmetry of the embedded pyramidal dot results in a much richer strain profile.[13] The tip of the pyramid expands in the horizontal directions ($\epsilon_{xx}, \epsilon_{yy}$), but is compressed in the vertical direction (ϵ_{zz}). At the base of the pyramid, the InAs dot is constrained to adopt the GaAs substrate lattice constant, which results in compression in the horizontal directions ($\epsilon_{xx}, \epsilon_{yy}$), and a compensating expansion in the vertical direction (ϵ_{zz}).

B. Strain-modified confining potentials

The effect of the above strain profiles on the electronic structure of the dots can be qualitatively understood by examining the strain-modified band offsets. These can be approximately calculated by coupling the electron and hole band edges to their deformation potentials. The electron band edge E_c couples only to the sum of the diagonal strain components,

$$E_c(\epsilon) = a_c(\epsilon_{xx} + \epsilon_{yy} + \epsilon_{zz}), \tag{7}$$

where a_c is the deformation potential of the conduction band at the Γ_{1c} point. The heavy- and light-hole band edges, E_{hh} and E_{lh}, couple to the individual strain components[19] according to

$$E_{hh}(\epsilon) = \frac{1}{3}(\Delta^{SO} + \Delta^{CF}),$$

$$E_{lh}(\epsilon) = -\frac{1}{6}(\Delta^{SO} + \Delta^{CF}) + \frac{1}{2}\sqrt{(\Delta^{SO} + \Delta^{CF})^2 - \frac{8}{3}\Delta^{SO}\Delta^{CF}}, \tag{8}$$

where the crystal field splitting $\Delta^{CF}(\epsilon)$ is defined as $-3b(\epsilon_{zz} - \epsilon_{xx})$, and b is the biaxial deformation potential, and Δ^{SO} is the spin-orbit splitting. Our fitted values for a_c and b are 7.12 meV Kbar^{-1} and -1.85 eV, respectively. We emphasize that Eqs. (7) and (8) and Fig. 2 are only used for illustration purposes. The full pseudopotential calculations (see Figs. 3 and 4 below) directly include the strain in the Hamiltonian for the system and are completely separate to the approximate band offsets shown in Fig. 2.

The strain-modified band edges of the GaAs-embedded (a) spherical and (b) pyramidal InAs dots, calculated using Eqs. (7) and (8), are illustrated in Fig. 2, which shows the

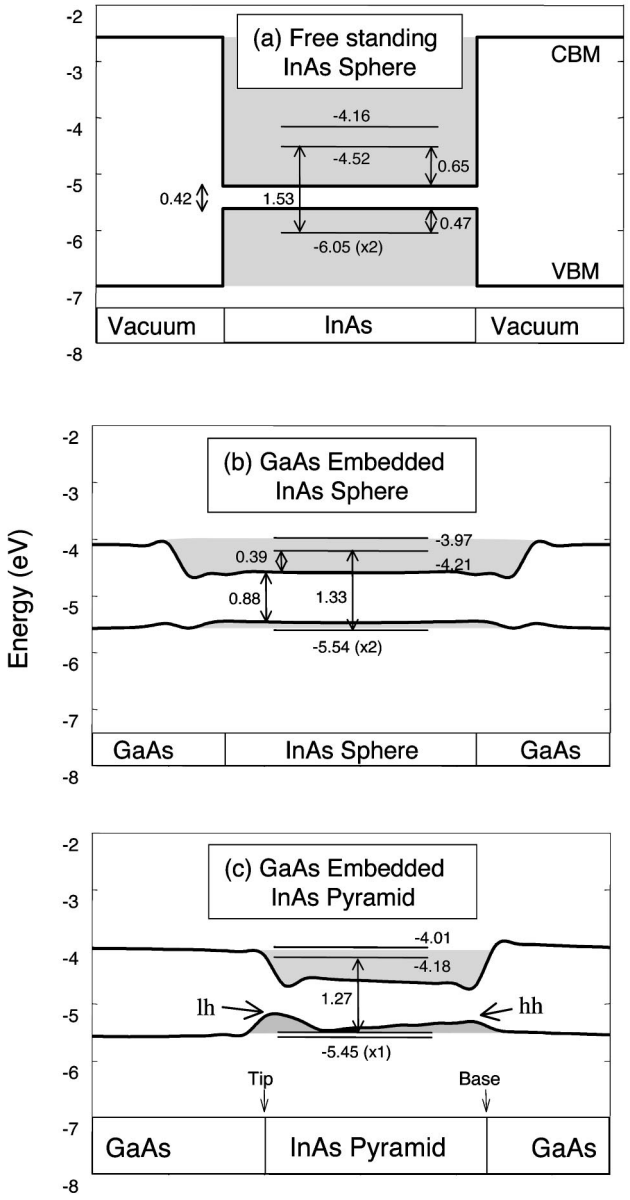

FIG. 3. Strain modified potential offsets for the CBM and VBM along a [001] line through the center of each dot. These are obtained by calculating the pseudopotential bulk band structures of InAs and GaAs in a supercell geometry, using the local strain of the dot (Fig. 1). The InAs/vacuum and InAs/GaAs offsets are shaded gray. The horizontal lines mark the energies of the confined electron and hole levels in the dots. These levels are calculated by using the folded spectrum method to find the band-edge eigenstates of the empirical pseudopotential Hamiltonian [Eq. (1)]. All states are singly degenerate except where marked in brackets.

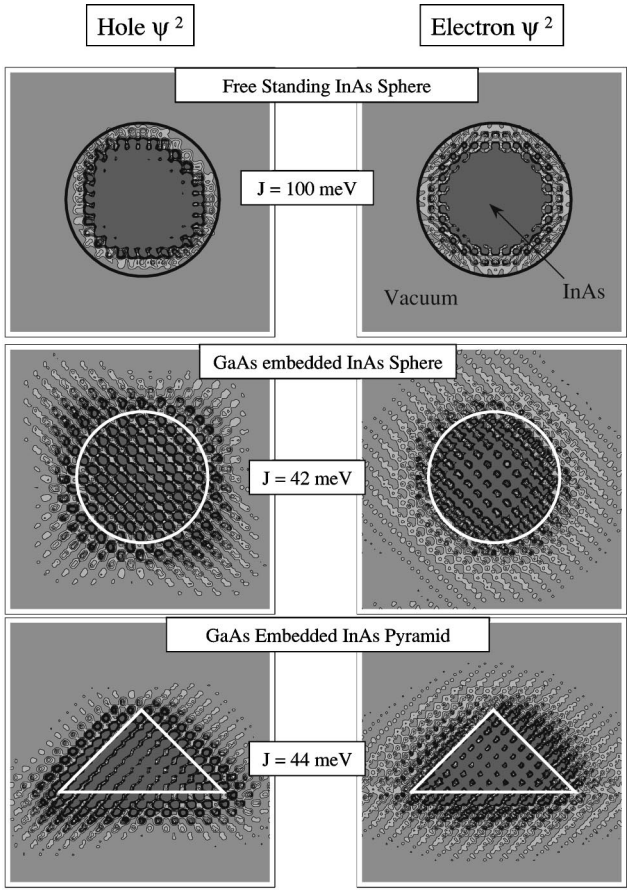

FIG. 4. Contour plots of the electron and hole wave functions in the {010} plane through the center of all three dots.

electron (E_c), heavy-hole, and light-hole (E_{hh},E_{lh}) potential offsets in the {010} plane through the center of the dots. For both the spherical and pyramidal geometries, the InAs dots act as wells for both electrons and holes. In the spherical dot the confining wells are flat bottomed and adopt the spherical symmetry of the dot. In the lower symmetry, pyramidal case the wells are no longer flat-bottomed. The pyramidal electron well has two peaks, one near the tip and one near the base of the pyramid [see also below in Fig. 3(c)]. The pyramidal heavy- and light-hole wells have peaks at the base and tip, respectively [indicated by arrows in Fig. 2(b)]. The location of these peaks is implied by Fig. 1(b), which shows that $[\epsilon_{zz}-\epsilon_{xx}]$, and hence the crystal field splitting Δ^{CF} changes sign from positive at the base of the pyramid ($\epsilon_{zz}>\epsilon_{xx}$) to negative at the tip ($\epsilon_{zz}<\epsilon_{xx}$). This change in sign results in the observed heavy-hole peak at the base of the pyramid ($\Delta^{CF}>0$) and light-hole peak at the tip of the pyramid ($\Delta^{CF}<0$). Thus we expect that in the embedded spherical dot, electrons and holes will be attracted to the center of the dot, while in the pyramidal dot, electrons will also be attracted to the center of the dot but heavy holes will be attracted to the base of the pyramid and light holes attracted to the tip.

A more accurate picture of the strain-modified band edges can be obtained by calculating the energies of the bulk valence-band maximum (VBM) and conduction-band maximum (CBM) using our full pseudopotential subjected to the *local* strain produced by the dot. Figure 3 shows as thick lines the strain modified bulk band edges (on an absolute scale with respect to vacuum) of the lowest energy conduction and highest energy valence states along a [001] line through the center of each of the three dot systems. These band edge energies are obtained by performing a series of *bulk* calculations using the local strain in the dot, $\epsilon(\mathbf{R})$, at a series of points along the line **R**. Within the small strain regime where deformation potential theory is applicable, the energy of the CBM's in Fig. 3 correspond to the electron band edges in Fig. 2, while the energy of the highest hole

corresponds to the heavy hole for the spherical dots and a combination of the heavy hole near the base and light hole near the tip for the pyramidal dot.

The two lowest confined electron and highest hole energy levels of the Hamiltonian in Eq. (1) are plotted as thin horizontal lines. These were calculated using the folded spectrum method [Eq.(5)] where the reference energy ϵ_{ref} was placed in the band gap of the dots. For the electron levels, the reference energy was set to -4.5 eV and a total of four eigenstates were calculated (excluding spin degeneracy). For the hole levels, the reference energy was set to -5.2 eV and a total of eight eigenstates were calculated (excluding spin degeneracy). Comparison of the free-standing sphere (a), and the embedded sphere (b), reveals that two separate effects control how the confined energy levels shift upon embedding the dot in GaAs. Firstly, the large conduction- and valence-band offsets (shaded gray) between InAs and ''vacuum'' result in a larger quantum confinement of the confined electrons and holes (0.65 and 0.47 eV) in the free-standing dots than in the GaAs-embedded dots (0.39 and 0.07 eV). However, the compressive strain in the embedded InAs dot widens the InAs band gap from 0.42 to 0.88 eV. This pushes the electron level in the embedded dot (-4.205 eV) above that of the free-standing dot (-4.517 eV), even though the quantum confinement is smaller. When the effects of quantum confinement and strain induced level shifts are combined, the confined hole to confined electron gap of the free-standing sphere (1.532 eV) is 0.198 eV *larger* than that of the same sized embedded sphere (1.334 eV).

Comparing the embedded sphere (b), with the embedded pyramid (c), one sees that the lower symmetry of the pyramidal geometry results in a richer strain-modified band edge profile showing distinct peaks near the tip and the base. The pyramidal wave function localizes within these lower energy peaks, hence reducing its energy with respect to that of the spherical dot. The electron and hole energies in the pyramid are 0.021 and 0.086 eV lower and higher, respectively, than those in the spherical embedded dot, producing a confined hole to confined electron gap (1.269 eV) that is 0.065 eV smaller than that of the comparably sized GaAs embedded spherical dot. The lower symmetry of the pyramid also splits the degeneracy of the VBM which is doubly degenerate in the spherical geometry.

C. Wave functions of confined state and electron-hole Coulomb energies

Figure 4 shows contour plots of the confined hole and confined electron wave functions squared in the {010} plane through the center of all three dots (same plane as Fig. 2). The plots show that the hole and electron wave functions in all three dots have envelope functions with *s* symmetry, with the wave function localized within the InAs dots. However, the significantly smaller GaAs/InAs band offsets result in less wave-function localization in the GaAs-embedded InAs dots than in the free-standing dot. We find 94.9% and 90.5% of the VBM and CBM wave-function amplitudes contained within the free-standing dot, compared to 42.2% and 58.4% in the embedded sphere and 52.6% and 46.9% in the embedded pyramid. The ''spillage'' of the wave functions out of the embedded dots can be clearly seen in the contour plots in Fig. 4. The energetic consequence of the stronger wave-function localization inside the free-standing dot can be seen by calculating the screened electron-hole Coulomb energy J_{eh} defined as

$$J_{eh}=\int\int \frac{|\psi_e(\mathbf{r}_1)|^2|\psi_h(\mathbf{r}_2)|^2}{\bar{\epsilon}(\mathbf{r}_1-\mathbf{r}_2)|\mathbf{r}_1-\mathbf{r}_2|}d\mathbf{r}_1 d\mathbf{r}_2, \tag{9}$$

where $\psi_{e,h}$ are the electron and hole wave functions and $\bar{\epsilon}$ is a screened dielectric function[20] containing a Thomas-Fermi electronic component and an ionic component from Ref. 21. As a result of the increased wave-function localization, we find a stronger electron-hole Coulomb energy (0.100 eV) in the free-standing dot than in the GaAs-embedded spherical dot (0.042 eV) and the GaAs-embedded pyramidal dot (0.044 eV). The lowest excitonic transition E_{e-h} defined as

$$E_{e-h}=(\epsilon_e-\epsilon_h)-J_{eh}, \tag{10}$$

where $\epsilon_{e,h}$ are the single particle energies of the confined electron and hole are

$$\begin{aligned} E_{eh}(\text{free-standing sphere})&=1.532-0.100=1.432\,\text{eV},\\ E_{eh}(\text{GaAs-embedded sphere})&=1.334-0.040=1.294\,\text{eV},\\ E_{eh}(\text{GaAs-embedded pyramid})&=1.269-0.044=1.225\,\text{eV}, \end{aligned} \tag{11}$$

D. Polarization of interband transitions

The dipole matrix transition probability for transitions from confined hole to confined electron states $M_{h\to e}$ were calculated according to

$$M_{h\to e}=|\langle\psi_h|\nabla|\psi_e\rangle|^2. \tag{12}$$

The transition dipole matrix elements between the highest three hole states (h_1 to h_3) and the lowest three electron states (e_1 to e_3) in each of the dots are given in Table II for polarizations along the [110], [$\bar{1}$10], and [001] directions. Where degeneracies exist, the matrix elements are summed over the degenerate states. The total transition probability, *M*, for the fundamental h_1 to e_1 transition is 25.5% of the calculated bulk InAs value for the free-standing InAs dot, compared to 50.8% and 60.8% for GaAs-embedded sphere and pyramid, respectively. The larger transition probabilities for the embedded dots compared to the free-standing dot is again consistent with the more delocalized nature of the electron and hole wave functions in these embedded dots. Table II shows that the dipole matrix elements of the spherical free-standing and embedded dots [(a) and (b)] along [110], [$\bar{1}$10], and [001] are identical. However, the inequivalence of the (101) and (011) facets of a pyramid constructed from a zinc-blende material lead to a lower C_{2v} symmetry and this in turn produces different [110] and [$\bar{1}$10] matrix elements in the pyramid. One also sees that the matrix elements decrease dramatically for transitions between states farther from the gap.

The similarity in wave-function localization, Coulomb energies, and transition probabilities between the embedded spherical and embedded pyramidal dots suggest that the elec-

TABLE II. Transition dipole matrix elements as defined in Eq. (12), between the highest three valence states (h_1 to h_3) and the lowest three electron states (e_1 to e_3) for a (a) free-standing spherical InAs dot (diameter 42.2 Å), (b) the same InAs dot embedded in GaAs, and (c) pyramidal InAs dot with 30.3 Å height and 60.6 Å base embedded in GaAs. Matrix elements are given for light polarized along [110] , [$\bar{1}$10], and [001]. All values are given as fractions of the calculated bulk InAs transition probability.

		e_1			e_2			e_3		
		[110]	[$\bar{1}$10]	[001]	[110]	[$\bar{1}$10]	[001]	[110]	[$\bar{1}$10]	[001]
	(a)	0.085	0.085	0.085	0.023	0.023	0.023	0.000	0.000	0.000
h_1	(b)	0.170	0.168	0.170	0.001	0.001	0.001	0.020	0.022	0.021
	(c)	0.317	0.291	0.000	0.001	0.004	0.014	0.002	0.001	0.000
	(a)	0.043	0.043	0.043	0.046	0.046	0.046	0.000	0.000	0.000
h_2	(b)	0.070	0.071	0.070	0.002	0.002	0.002	0.037	0.039	0.038
	(c)	0.008	0.001	0.002	0.098	0.082	0.000	0.004	0.000	0.000
	(a)	0.002	0.002	0.002	0.003	0.001	0.002	0.000	0.000	0.000
h_3	(b)	0.002	0.002	0.002	0.001	0.001	0.001	0.033	0.023	0.027
	(c)	0.028	0.096	0.112	0.026	0.019	0.005	0.009	0.000	0.005

tronic structure of the dots is strongly affected by the size of the band offsets, but not so strongly affected by their geometry.

IV. SUMMARY

We have performed fully atomistic, pseudopotential calculations of free-standing and GaAs-embedded, spherical and pyramidal InAs quantum dots. The valence- and conduction-band offsets between the free-standing InAs dot and vacuum are much larger than between GaAs and the embedded InAs dots. The larger offsets in the free-standing system produce greater quantum confinement of the energy levels and therefore a larger confined electron to a confined hole band gap. They also increase the localization of the electron and hole wave functions within the dot, which in turn increases the electron-hole Coulomb energy and decreases the electron-hole dipole transition matrix element. The lower symmetry of the pyramidal dot, produces a richer strain profile than the spherical dots, that splits the degeneracy of the VBM states, reduces the quantum confinement of the wave functions still further and polarizes the emitted light.

ACKNOWLEDGMENTS

This work was supported by the DOE, Basic Energy Sciences, Division of Materials Science under Contract No. DE-AC36-83CH10093. The authors thank L.W. Wang and S.H. Wei for useful discussions.

[1] N. Carlsson *et al.*, J. Cryst. Growth **170**, 1271 (1997).
[2] K. Schmidt, G. Medeiros-Ribeiro, M. Oestreich, and P. Petroff, Phys. Rev. B **54**, 11 346 (1996).
[3] G. Solomon, J. Trezza, A. Marshall, and J. Harris, Phys. Rev. Lett. **76**, 952 (1996).
[4] N. Carlsson, W. Seifert, A. Petersson, P. Castrillo, M. E. Pistol, and L. Samuelson, Appl. Phys. Lett. **66**, 3093 (1994).
[5] A. Henglein, Chem. Rev. **89**, 1861 (1998).
[6] L. Brus, J. Phys. Chem. Solids **59**, 459 (1998).
[7] D. Norris and M. Bawendi, Phys. Rev. B **53**, 16 338 (1996).
[8] M. Chamarro, V. Voliotis, R. Grousson, P. Lavallard, T. Gacoin, G. Counio, J. P. Boilot, and R. Cases, J. Cryst. Growth **159**, 853 (1995).
[9] D. Bertram, O. Micic, and A. Nozik, Phys. Rev. B **57**, R4265 (1998).
[10] U. Banin, J. C. Lee, A. A. Guzelian, V. Kadavanich, A. P. Alivisatos, W. Jaskolski, G. W. Bruant, Al. L. Efros, and M. Rosen, J. Chem. Phys. **109**, 2306 (1998).
[11] L.-W. Wang and A. Zunger, Phys. Rev. B **51**, 17 398 (1995).
[12] P. Keating, Phys. Rev. **145**, 637 (1966).
[13] C. Pryor, J. Kim, L.-W. Wang, A. Williamson, and A. Zunger, J. Appl. Phys. **83**, 2548 (1998).
[14] R. Martin, Phys. Rev. B **1**, 4005 (1970).
[15] A. Silverman, A. Zunger, R. Kalish, and J. Adler, J. Chem. Phys. **100**, 2394 (1994).
[16] L.-W. Wang and A. Zunger, J. Chem. Phys. **100**, 2394 (1994).
[17] L.-W. Wang and A. Zunger, *Semiconductor Nanoclusters* (Elsevier Science, Amsterdam, 1996).
[18] J. Eshelby, J. Appl. Phys. **25**, 255 (1954).
[19] S.-H. Wei and A. Zunger, Phys. Rev. B **49**, 14 337 (1994).
[20] A. Williamson and A. Zunger, Phys. Rev. B **58**, 6724 (1998).
[21] H. Haken, Nuovo Cimento **10**, 1230 (1956).